

## Stable Room-Temperature Molecular Negative Differential Resistance Based on Molecule–Electrode Interface Chemistry

Adi Salomon,<sup>†</sup> Rina Arad-Yellin,<sup>‡</sup> Abraham Shanzer,<sup>‡</sup> Amir Karton,<sup>‡</sup> and David Cahen<sup>\*†</sup>

Contribution from the Departments of Materials & Interfaces and Organic Chemistry, Weizmann Institute of Science, Rehovot 76100, Israel

Received January 23, 2004; E-mail: david.cahen@weizmann.ac.il.

**Abstract:** We show reproducible, stable negative differential resistance (NDR) at room temperature in molecule-controlled, solvent-free devices, based on reversible changes in molecule–electrode interface properties. The active component is the cyclic disulfide end of a series of molecules adsorbed onto mercury. As this active component is reduced, the Hg–molecule contact is broken, and an insulating barrier at the molecule–electrode interface is formed. Therefore, the alignment of the molecular energy levels, relative to the Fermi levels of the electrodes, is changed. This effect results in a decrease in the current with voltage increase as the reduction process progresses, leading to the so-called NDR behavior. The effect is reproducible and repeatable over more than 50 scans without any reduction in the current. The stability of the system, which is in the “solid state” except for the Hg, is due to the molecular design where long alkyl chains keep the molecules aligned with respect to the Hg electrode, even when they are not bound to it any longer.

### 1. Introduction

Understanding how electronic charge crosses molecules is a fundamental step in the development of molecule-based electronics. It has recently become apparent that molecule–electrode interface properties can dominate charge transport through molecules and can partially or fully screen the electronic transport properties of the molecule itself.<sup>1–4</sup> The electronic properties of the molecule–electrode interface are determined by the presence or absence of a chemical bond between the molecule and the electrode and the nature of such a bond. This bond determines the dipole at the molecule–electrode interface and the resulting potential drop along this interface, which, in turn, governs the alignment of the molecular levels, relative to the Fermi levels of the electrodes. Indeed, it was found experimentally that for otherwise identical systems, the absence of a chemical bond at the molecule–electrode interface can reduce charge transport efficiency across the molecule-based junction by orders of magnitude.<sup>5–10</sup>

Furthermore, similar to what is known for nonmolecular inorganic metal/semiconductor junctions,<sup>11</sup> a layer of polar molecules at the metal/semiconductor interface can change the barrier height for electron transport across that interface.<sup>12,13</sup>

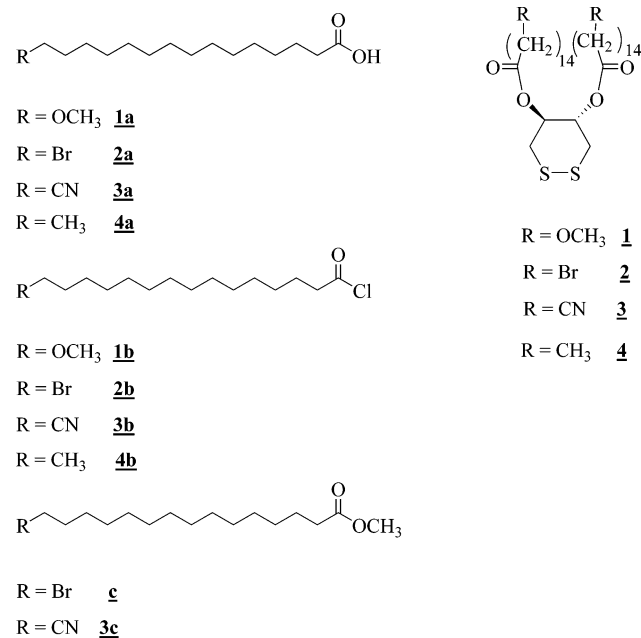
Experimentally, several examples have been reported of NDR in electrode–molecule–electrode junctions. Following inorganic semiconductor-based NDR, resonant tunneling has been taken to be the main route to molecular NDR for metal/molecule/metal,<sup>14–16</sup> and metal/molecule/semiconductor<sup>17,18</sup> systems. Since resonant tunneling requires conjugated molecules with a relatively low energy gap, or molecules with an electroactive group,<sup>16,19</sup> the emphasis was on the electrical properties of the molecule itself.<sup>14,20–24</sup> As interface properties may mask the molecule’s signature, one can argue that the problem in

<sup>†</sup> Department of Materials & Interfaces.

<sup>‡</sup> Department of Organic Chemistry.

- (1) Cahen, D.; Hodes, G. *Adv. Mater.* **2002**, *11*, 789–798.
- (2) Heath, J. R.; Ratner, M. A. *Physics Today* **2003**, *May*, 43–49.
- (3) Hipps, K. W. *Science* **2001**, *294*, 535–537.
- (4) Stewart, D. R.; Ohlberg, D. A. A.; Beck, P. A.; Chen, Y.; Williams, S. R. *Nano Lett.* **2004**, *4*, 133–136.
- (5) Cui, X. D.; Primak, A.; Zarate, X.; Tomfohr, J.; Sankey, O. F.; Lindsay, S. M. *Science* **2001**, *294*, 571–574.
- (6) Selzer, Y.; Salomon, A.; Cahen, D. *J. Phys. Chem. B* **2002**, *106*, 10432–10439.
- (7) Salomon, A.; Cahen, D.; Lindsay, S.; Tomfohr, J.; Engelkes, V.; Frisbie, C. D. *Adv. Mater.* **2003**, *15*, 1881–1890.
- (8) Beebe, J. M.; Engelkes, V. B.; Miller, L. L.; Frisbie, C. D. *J. Am. Chem. Soc.* **2002**, *124*, 11268.
- (9) Kushmerick, J. G.; Holt, D. B.; Yang, J. C. *Phys. Rev. Lett.* **2002**, *89*, 086802–086801.
- (10) Tivanski, A. V.; He, Y.; Liu, H.; Walker, G. C.; Waldeck, D. H. submitted.
- (11) Tung, R. T. *Phys. Rev. Lett.* **2000**, *84*, 6078–6081.
- (12) Vilan, A.; Shanzer, A.; Cahen, D. *Nature* **2000**, *404*, 166–168.
- (13) Salomon, A.; Berkovich, D.; Cahen, D. *Appl. Phys. Lett.* **2003**, *82*, 1051–1053.
- (14) Wassel, R. A.; Credo, G. M.; Fuierer, R. R.; Feldheim, D. L.; Gorman, C. B. *J. Am. Chem. Soc.* **2004**, *126*, 295–300.
- (15) Karzazi, Y.; Cornil, J.; Bredas, J. L. *Nanotechnology* **2002**, *13*, 336.
- (16) Chen, J.; Reed, M. A.; Rawlett, A. M.; Tour, J. M. *Science* **1999**, *286*, 1550–1551.
- (17) Rakshit, T.; Liang, G. C.; Ghosh, W. A.; Datta, S. *Phys. Rev. Lett.* **2004**, in press.
- (18) Guisinger, N. P.; Greene, M. E.; Basu, R.; Baluch, A. S.; Hersam, M. C. *Nano Lett.* **2004**, *4*, 55–59.
- (19) Gorman, C. B.; Carroll, R. L.; Fuierer, R. R. *Langmuir* **2001**, *17*, 6923–6930.
- (20) Zeng, C.; Wang, H.; Yang, J.; Hou, J. G. *Appl. Phys. Lett.* **2000**, *77*, 3595–3597.
- (21) Chen, J.; Wang, H.; Reed, M. A. *Appl. Phys. Lett.* **2000**, *77*, 1224–1226.
- (22) Kratochvilova, I.; Kocirik, M.; Zambova, A.; Mbindyo, J.; Mallouk, T. E.; Mayer, T. S. *J. Mater. Chem.* **2002**, *12*, 2927–2930.
- (23) Fan, F. R. F.; Yang, J. P.; Cai, L. T.; Price, D. W.; Dirk, S. M.; Kosynkin, D. V.; Yao, Y. X.; Rawlett, A. M.; Tour, J. M.; Bard, A. J. *J. Am. Chem. Soc.* **2002**, *124*, 5550–5560.
- (24) Le, J. D.; He, J.; Hoye, T. R.; Mead, C. C.; Kiehl, R. A. *Appl. Phys. Lett.* **2003**, *83*, 5518–5520.

**Scheme 1.** Molecular Structure of the 1,2-Dithiane Derivatives and the Synthetic Steps Used for the Preparation of These Compounds



achieving stable molecular solid-state NDR at room temperature is due to interface properties that are apparently difficult to control.

Because of the importance of the molecule–electrode interface for charge transport, we explored the possibility to use both the molecule–electrode contact and molecular dipole effects for device action. In a preliminary communication, we have shown that one can build a molecular controlled device that shows large NDR at room temperature, which varies systematically with the molecular dipole at the metal/semiconductor interface. However, this NDR was not stable and disappeared permanently after 1–2 scans.<sup>25</sup> Now we report on a stable, reproducible, room-temperature molecular NDR. The phenomenon is based on the chemistry at the molecule–electrode interface, more specifically, the possibility to control the chemical bond at the molecule–electrode interface. The stability of the system is due to molecular design, which is based on what we have learned from our earlier work.

## 2. Experimental Section

**2.1. Syntheses. 2.1.1. General.** Chemicals and reagents were purchased from Sigma. All solvents were dried before use. Chloroform and methylene chloride were passed through a basic alumina column. Tetrahydrofuran was distilled from Na under argon. Pyridine was dried over KOH and distilled.

The <sup>1</sup>H NMR spectra were measured on an Avance DPX-400 MHz or DPX-250 MHz spectrometers (Bruker) using the solvent's deuterium signal as the internal reference. IR spectra were recorded on a Protégé 460 FTIR spectrometer and the Mass Spectrometer Instrument used was the Micromass Platform LCZ 4000, (Micromass, Manchester, United Kingdom). The ionization mode was ESI.

The molecular structure of the different compounds and the synthetic steps are summarized in Scheme 1.

**2.1.2. Diester of 15-Methoxy-pentadecanoic Acid and 1,2-Dithiane-4,5-diol (1).** The compound was prepared following several steps.

**2.1.2.1. 15-Methoxy-pentadecanoic Acid (1a).** A small chip of sodium (approximately 100 mg) was added to a three-necked flask equipped with a magnetic stirrer, a reflux condenser, and a drying tube. The mixture was stirred at room temperature until all sodium was dissolved. To this was added 15-bromopentadecanoic acid (**2a**, Scheme 1, 300 mg, 0.93 mmol) dissolved in THF (5 mL), followed by NaI (25 mg), and the solution was refluxed for 8 h. The solvents were removed; water (20 mL) was added, and a 1 N KHSO<sub>4</sub> solution was added to change the pH to 1. Extraction with ether (3 × 20 mL), drying over MgSO<sub>4</sub>, and removal of the ether afforded 250 mg (95%) of the product as white crystals; mp 48–50 °C.

<sup>1</sup>H NMR (CDCl<sub>3</sub>) δ = 3.24 (s, 3H, OCH<sub>3</sub>); 3.38 (t, *J* = 4.5 Hz, 2H, CH<sub>2</sub>OCH<sub>3</sub>); 2.33 (t, *J* = 6.75 Hz, 2H, CH<sub>2</sub>COOH); 1.60–1.55 (m, 4H, CH<sub>2</sub>CH<sub>2</sub>OCH<sub>3</sub> + CH<sub>2</sub>CH<sub>2</sub>COOH); 1.35–1.20 (m, 20H, (CH<sub>2</sub>)<sub>10</sub>). MS–ES (*m/z*): = 272.19.

**2.1.2.2. 15-Methoxy-pentadecanoyl Chloride (1b).** 15-Methoxy-pentadecanoic acid (**1a**, Scheme 1, 250 mg) was dissolved in chloroform (5 mL). Oxalyl chloride (700 μL) and dimethylformamide (1 drop) were added and the solution was stirred overnight at room temperature. The solvent was removed and the residue was identified as the acyl chloride by IR.

IR (CDCl<sub>3</sub>) ν = 2932, 2863, 2250, 1800, 1672, 1461, 1113 cm<sup>-1</sup>.

**2.1.2.3. 15-Methoxy-pentadecanoic Acid 5-(15-Methoxy-pentadecanoyloxy)-1,2-dithian-4-yl Ester (1).** 15-Methoxy-pentadecanoyl chloride (**1b**, Scheme 1, 250 mg, 0.86 mmol) was dissolved in chloroform (5 mL) and was cooled in an ice-bath. 1,2-dithiane-4,5-diol (50 mg, 0.39 mmol) in pyridine (0.5 mL) was added and the solution was stirred for 30 min in the cold and for 2 days at room temperature. Chloroform (20 mL) was added and the solution was washed with 1 N HCl, water, 1 N NaHCO<sub>3</sub>, and brine. The solution was dried over MgSO<sub>4</sub> and the solvent was removed. The residue (192 mg) was purified by column chromatography on silica gel using a CHCl<sub>3</sub>:hexane 7:3 solution as eluent. Fractions of 10 mL each were collected and the product (84.8 mg, 33% yield) was isolated from fractions 15–20; mp 58–60 °C.

<sup>1</sup>H NMR (CDCl<sub>3</sub>) δ = 5.018, 4.992 (2d *J* = 4.75, 2H, CHO); 3.32 (s, 6H, OCH<sub>3</sub>); 3.35 (t, *J* = 6.5 Hz, 4H, CH<sub>2</sub>OCH<sub>3</sub>); 3.20–2.95 (m, 4H, CH<sub>2</sub>S); 2.25 (t, *J* = 7.5 Hz, 4H, CH<sub>2</sub>COO); 1.55–1.50 (m, 8H, CH<sub>2</sub>-CH<sub>2</sub>OCH<sub>3</sub> + CH<sub>2</sub>CH<sub>2</sub>COOH); 1.30–1.20 (m, 40H, (CH<sub>2</sub>)<sub>10</sub>).

**2.1.3. Diester of 15-Bromo-pentadecanoic Acid and 1,2-Dithiane-4,5-diol (2).** **2.1.3.1. 15-Bromo-pentadecanoyl Chloride (2b).** 15-Bromopentadecanoic acid (**2a**, Scheme 1, 250 mg) was dissolved in chloroform (5 mL). Oxalyl chloride (700 μL) and dimethylformamide (1 drop) were added and the solution was stirred overnight at room temperature. The solvent was removed and the residue was identified as the acyl chloride by IR.

IR (CDCl<sub>3</sub>) ν = 2932, 2851, 1796, 1461 cm<sup>-1</sup>.

**2.1.3.2. 5-(15-Bromo-pentadecanoyloxy)-1,2-dithian-4-yl 15-Bromo-pentadecanate (2).** The compound was prepared following a similar protocol to that described for **1**. Purification was achieved by column chromatography on silica gel using 2% ethyl acetate in CH<sub>2</sub>-Cl<sub>2</sub> as eluent. Fractions of 10 mL each were collected and the product was isolated from fractions 15–20 in 30% yield. Mp 55–57 °C.

<sup>1</sup>H NMR (CDCl<sub>3</sub>) δ = 5.032, 4.99 (2d, *J* = 4.6, 2H, CHO); 3.32 (s, 6H, OCH<sub>3</sub>); 3.40 (t, *J* = 6.8 Hz, 4H, CH<sub>2</sub>OCH<sub>3</sub>); 3.20–2.95 (m, 4H, CH<sub>2</sub>S); 2.27 (t, *J* = 7.8 Hz, 4H, CH<sub>2</sub>COO); 1.64–1.54 (m, 4H, CH<sub>2</sub>-CH<sub>2</sub>Br); 1.55–1.50 (m, 4H, CH<sub>2</sub>CH<sub>2</sub>COO); 1.30–1.20 (m, 40H, (CH<sub>2</sub>)<sub>10</sub>). MS–ES (*m/z*): 758, with the typical pattern of two bromine atoms 758.24 (100.0%), 760.24 (55.1%), 756.25 (49.2%), 759.25 (37.5%), 761.24 (21.7%), 757.25 (19.9%).

**2.1.4. 5-(15-Cyano-pentadecanoyloxy)-1,2-dithian-4-yl 15-Cyano-pentadecanate (3).** **2.1.4.1. 15-Cyano-pentadecanoic acid (3a).** Four steps were followed:

**A. Methyl 15-Bromo-pentadecanate (c).** Methanol (2 mL) was added to a solution of 15-bromo-pentadecanoic acid (**2a** Scheme 1, 0.5 g, 1.5 mmol) in THF (7 mL). Trimethylsilyl diazomethane (1.7

(25) Selzer, Y.; Salomon, A.; Ghabboun, J.; Cahen, D. *Angew. Chem., Int. Ed.* **2002**, *41*, 827–830.

mL, 2 N solution in hexane) was added and the solution was stirred at room temperature for 2 h. The solvents were removed, the residue was dissolved in chloroform, the solution was washed with water and with brine and dried over  $MgSO_4$ , and the solvent was removed. The methyl ester (486 mg) was obtained as oil in 94% yield.

$^1H$  NMR ( $CDCl_3$ )  $\delta$  = 3.66 (s, 3H,  $OCH_3$ ); 3.43 (t,  $J$  = 6.8 Hz, 2H,  $CH_2Br$ ); 2.30 (t,  $J$  = 7.4 Hz, 2H,  $CH_2COOMe$ ); 1.84 (q,  $J$  = 7.4 Hz, 2H,  $CH_2CH_2COOCH_3$ ); 1.55–1.50 (m, 2H,  $CH_2CH_2COO$ ); 1.30–1.20 (m, 20H,  $(CH_2)_{10}$ ).

**B. 15-Cyano-pentadecanoate.** Methyl 15-cyano-pentadecanoate (**3c**) was prepared following a protocol similar to that described by Lu et al.<sup>26</sup>

Methyl 15-bromo-pentadecanoate (**c**, 485 mg, 1.45 mmol) was dissolved in acetonitrile (30 mL). KCN (280 mg, 4.3 mmol) and 18-crown-6 (53 mg, 0.20 mmol) were added and the two-phase system was stirred under reflux for 40 h. The reaction mixture was cooled to room temperature and the solvent evaporated. The residue was suspended in water (15 mL) and extracted with ether ( $4 \times 10$  mL); the ether extract was dried over  $Na_2SO_4$  and the solvent was evaporated. The product (400 mg) was obtained as colorless oil.

$^1H$  NMR ( $CDCl_3$ )  $\delta$  = 3.65 (s, 3H); 2.35 (t,  $J$  = 7.1 Hz, 2H,  $CH_2CN$ ); 2.29 (t,  $J$  = 7.7 Hz, 2H,  $CH_2CO_2CH_3$ ); 1.65 (m, 2H); 1.45 (m, 2H); 1.3 (s, 20H).

**C. 15-Cyano-pentadecanoic Acid (3a).** Methyl 15-cyano-pentadecanoate (**3c**, 300 mg, 1.7 mmol) was dissolved in 10 mL of methanol/tetrahydrofuran (1:1). To this was added  $LiOH \cdot H_2O$  (750 mg) and the reaction mixture was refluxed for 5 h. The solvent was removed and the residue was dissolved in water (20 mL) and extracted with ether ( $3 \times 10$  mL). The aqueous layer was acidified to pH 1 and extracted with ether ( $4 \times 10$  mL). The solution was dried over  $Na_2SO_4$ , the solvent was evaporated, and the crude product (250 mg) was obtained as colorless oil in 60% yield.

$^1H$  NMR ( $CDCl_3 + D_2O$ )  $\delta$  = 2.32 (t,  $J$  = 7.4 Hz, 2H,  $CH_2CN$ ); 2.33 (t,  $J$  = 7.1 Hz, 2H,  $CH_2CO_2H$ ); 1.67–1.61 (m, 2H); 1.45–1.3 (m, 22H). MS-ES<sup>-</sup> ( $m/z$ ): = 266.37.

**D. 15-Cyano-pentadecanoyl Chloride (3b).** 15-Cyano-pentadecanoyl chloride was prepared as described above.

IR (KBr  $CHCl_3$ ): 2928, 2856, 2257, 1794, 1459  $cm^{-1}$ .

**2.1.4.2. 5-(15-Cyano-pentadecanoyloxy)-1,2-dithian-4-yl 15-Cyano-pentadecanoate (3).** The compound was prepared following a similar protocol for the methoxy derivative (**1**) using 15-cyano-pentadecanoyl chloride (**3b**, prepared from 140 mg of **3a**, 0.5 mmol) and 1,2-dithiane-4, 5-diol (40 mg, 0.26 mmol). Purification was achieved by column chromatography on silica gel using  $CH_2Cl_2$  (400 mL) and  $CH_2Cl_2$ : MeOH 97:3 (300 mL) as eluents. Fractions of 5 mL each were collected and the product was isolated from fractions 80–115 in 30% yield. The product was crystallized from ethyl acetate–hexane; mp 70–72 °C.

$^1H$  NMR ( $CDCl_3$ ):  $\delta$  = 5.00, 4.98 (2d,  $J$  = 4.7, 2H,  $CHO$ ); 3.16–3.03 (m, 4H,  $CH_2S$ ); 2.32 (t,  $J$  = 7.0 Hz, 4H,  $CH_2CN$ ); 2.26 (t,  $J$  = 7.9 Hz, 4H,  $CH_2COO$ ); 1.64–1.54 (m, 4H,  $CH_2CH_2CN$ ); 1.55–1.50 (m, 4H,  $CH_2CH_2COO$ ); 1.40–1.20 (m, 40H,  $(CH_2)_{10}$ ). MS-ES<sup>+</sup> ( $m/z$ ): = 651.0.

**2.1.5. 5-(Hexadecanoyloxy)-1,2-dithian-4-yl Hexadecanoate (4).** The compound was prepared from 1, 2-dithiane-4, 5-diol (1 g, 2.3 mmol) and hexadecanoyl chloride (**4b**, Scheme 1, 1.25 g, 4.5 mmol) in dry  $CH_2Cl_2$ –pyridine solution as described above. Purification was achieved by column chromatography with (8:2)  $CH_2Cl_2$ :hexane solution as eluent. Fractions of 10 mL were collected and the product was recovered as white crystals from fractions 1–21; mp 48–50 °C.

$^1H$  NMR ( $CDCl_3$ ):  $\delta$  = 5.03, 5.1 (2d,  $J$  = 4.5 Hz, 2H,  $CHO$ ); 3.18–3.00 (m, 4H,  $CH_2S$ ); 2.27 (t,  $J$  = 7.6 Hz, 4H,  $CH_2COOH$ ); 1.58 (t,  $J$

= 7.5 Hz, 4H,  $CH_2CH_2COOH$ ); 1.30–1.24 (m, 40H,  $(CH_2)_{10}$ ); 0.88 (t,  $J$  = 7.0 Hz, 6H,  $CH_3$ ). MS-ES<sup>-</sup> ( $m/z$ ): = 629.93.

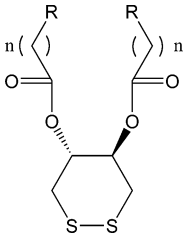
**2.2. Calculating the Dipole Moments of the Molecules.** The molecular dipole moments were calculated to get rough estimates of their relative magnitude. All calculations were done for the free, unbound molecules. They were done both for smaller molecules with four methylene groups, and for the molecules that were actually used. The reason was that for the small molecules we could use the energy-optimized geometries. These geometries were optimized by using Gaussian 03<sup>27</sup> at the B97-1/SDD level of theory. SDD is the combination of the Huzinaga–Dunning double- $\zeta$  basis set<sup>28</sup> on lighter elements with the Stuttgart–Dresden basis set-RECP combination<sup>29</sup> on bromine. The geometries of the full-length molecules were first optimized using the PM3 semiempirical method.<sup>30,31</sup> This led to geometries where the two alkyl chains point toward opposite directions so that van der Waals interactions between the chains are very unlikely. Therefore, the geometries were also manually adjusted based on experimental data and total energy considerations.<sup>32</sup> The energies of these geometries are higher by at most 50 kJ/mol than the PM3 semiempirical optimized geometry.<sup>33</sup> However, as this geometry allows for tight packing, this energy loss will easily be compensated for by the gains from van der Waals interactions.<sup>34</sup>

The dipole calculations for the experimentally used molecules ( $n$  = 14) were carried out using the Amsterdam Density Functional package (ADF2004.01),<sup>35–37</sup> using the Statistical Average of Orbital Potential (SAOP)<sup>36</sup> exchange-correlation functional in conjunction with a triple- $\zeta$  plus two polarization functions (TZ2P) Slater-type basis set. This functional has been used for the calculation of electronic properties of small molecules.<sup>36,38</sup>

The dipole moment calculations for the smaller molecules were also carried out at the B97-1/aug-cc-pVDZ level of theory. Aug-cc-pVDZ is the Dunning-augmented correlation consistent, polarized valence

- (27) Frisch, M. J.; Trucks, G. W.; Schlegel, H. B.; Scuseria, G. E.; Robb, M. A.; Cheeseman, J. R.; Montgomery, Jr. J. A.; Vreven, T.; Kudin, K. N.; Burant, J. C.; Millam, J. M.; Iyengar, S. S.; Tomasi, J.; Barone, V.; Mennucci, B.; Cossi, M.; Scalmani, G.; Rega, N.; Petersson, G. A.; Makatsuzki, H.; Hada, M.; Ehara, M.; Toyota, K.; Fukuda, R.; Hasegawa, J.; Ishida, M.; Nakajima, T.; Honda, Y.; Kitao, O.; Nakai, H.; Klene, M.; Li, X.; Knox, J. E.; Hratchian, H. P.; Cross, J. B.; Adamo, C.; Jaramillo, J.; Gomperts, R.; Stratmann, R. E.; Yazyev, O.; Austin, A. J.; Cammi, R.; Pomelli, C.; Ochterski, J. W.; Ayala, P. Y.; Morokuma, K.; Voth, G. A.; Salvador, P.; Dannenberg, J. J.; Zakrzewski, V. G.; Dapprich, S.; Daniels, A. D.; Strain, M. C.; Farkas, O.; Malick, D. K.; Rabuck, A. D.; Raghavachari, K.; Foresman, J. B.; Ortiz, J. V.; Cui, Q.; Baboul, A. G.; Clifford, Jr., S.; Cioslowski, J.; Stefanov, B. B.; Liu, G.; Liaskenko, A.; Piskorz, P.; Komaromi, I.; Martin, R. L.; Fox, D. J.; Keith, T.; Al-Laham, M. A.; Peng, C. Y.; Nanayakkara, A.; Challacombe, M.; Gill, P. M. W.; Johnson, B.; Chen, W.; Wong, M. W.; Gonzalez, C.; Pople, J. A. *Gaussian 03*, Revision B.02; Gaussian, Inc.: Pittsburgh, 2003.
- (28) Dunning, T. H. J.; Hay, P. J. In *Modern Theoretical Chemistry*, 3d ed.; Schaefer, H. F., Ed.; Plenum Press: New York, 1997; Vol. 4.
- (29) Dolg, M. In *Modern Methods and Algorithms of Quantum Chemistry*; Grotendort, J., Ed.; John von Neumann Institute for Computing: Jülich, 2000; Vol. 1, pp 479–508.
- (30) Stewart, J. J. P. *J. Comput. Chem.* **1989**, *10*, 209.
- (31) Stewart, J. J. P. *J. Comput. Chem.* **1989**, *10*, 221.
- (32) The geometry was adjusted so that the energy that the system gained by minimizing steric interactions and optimizing bond angles is compensated for by intermolecular van der Waals interactions between the  $CH_2$  groups. Such geometry optimization was based on the extensive earlier characterization of this type of molecules (with  $X = CH_3$ ) on Au (cf. Bruening et al.<sup>41</sup>), as we could not make such measurements for the molecules on Hg. Of special relevance were the ellipsometric thickness and the tilt angle of the alkyl chains relative to the surface normal.
- (33) The energies of the (free) molecules were calculated at the SAOP/TZ2P level of theory and were found to be between 15 and 50 kJ/mol higher than those with the PM3 optimized geometry.
- (34) Israelachvili, J. *Intermolecular & Surface Forces*, 2nd ed.; Elsevier: London, 1991.
- (35) Fonseca Guerra, C.; Snijders, J. G.; te Velde, G.; Baerends, E. J. *Theor. Chem. Acc.* **1998**, *99*, 391.
- (36) Schipper, P. R. T.; Gritsenko, O. V.; van Gisbergen, S. J. A.; Baerends, E. J. *J. Chem. Phys.* **2000**, *112*, 1344.
- (37) te Velde, G.; Bickelhaupt, F. M.; van Gisbergen, S. J. A.; Fonseca Guerra, C.; Baerends, E. J.; Snijders, J. G.; Ziegler, T. *J. Comput. Chem.* **2001**, *22*, 931–967.
- (38) Gruning, M.; Gritsenko, O. V.; Gisbergen, S. J. A. v.; Baerends, E. J. *J. Chem. Phys.* **2002**, *116*, 9591.

(26) Lu, P.; Alterman, M. A.; Chaurasia, C. S.; Bambal, R. B.; Hanzlik, R. P. *Arch. Biochem. Biophys.* **1997**, *337*, 1–7.

**Table 1.** Calculated Dipole Moments of the Free Molecules and for Their Smaller ( $n = 4$ ) Analogues<sup>a,b</sup>


R	dipole moments (D)		
	PM3 geometry $n = 14$	adjusted geometry $n = 14$	$n = 4$
Br	0.3	-0.3	-0.7
OCH <sub>3</sub>	-1.8	-3.0	-2.4
CN	3.6	4.1	3.5
CH <sub>3</sub>	-3.5	-4.8	-3.5

<sup>a</sup> For positive dipoles, the negative pole faces away from the Hg surface outward. <sup>b</sup> For the complete ( $n = 14$ ) molecules, the calculations were done for two geometries: one that was optimized using the PM3 semi-empirical method and another one that was manually adjusted, based on experimental data<sup>41</sup> and total energy calculations.

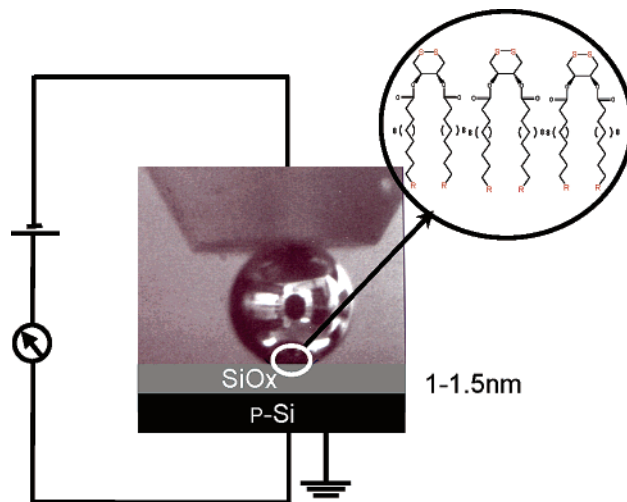
double- $\zeta$  basis set.<sup>39,40</sup> Table 1 shows the calculated dipole moments for all the cases discussed above. The data show that (a) the trend is the same for all cases and (b) in all cases, the Br derivative has the smallest absolute dipole moment, followed by the OCH<sub>3</sub> one.

For all calculations, the molecules have  $C_2$  symmetry. The dipole moments of the molecules with electron-donating end groups ( $R = \text{CH}_3, \text{OCH}_3$ ) always have signs opposite to that of the molecule with the strongest electron-withdrawing end groups ( $R = \text{CN}$ ). The difference in dipole moment of the  $R = \text{CH}_3$  and  $R = \text{OCH}_3$  derivatives can be ascribed to the C–O–C– bonding arrangement at the end of the  $R=\text{OCH}_3$  molecule. This reduces the polarity of the  $\text{H}_3\text{C}-(\text{CH}_2)_2-\text{C}(\text{O})-\text{O}-\text{C}-$  chains, compared to what is the case for the  $\text{H}_3\text{C}-(\text{CH}_2)_2-\text{C}(\text{O})-\text{O}-\text{C}-$  ( $R = \text{CH}_3$ ) chains.

**2.3. Sample Preparation.** Polished p-Si/SiO<sub>x</sub> <100> wafers with a nominal resistivity of  $1-10^{-3} \Omega\text{-cm}$ , were purchased from Virginia Semiconductors Ltd. Samples (1 cm<sup>2</sup>) were cleaned in a NH<sub>3</sub>:H<sub>2</sub>O<sub>2</sub>:H<sub>2</sub>O (1:1:5) solution at 70 °C for 10 min, followed by intensive rinsing for 30 s in DI water. The samples were put in a UV-ozonator for 7 min to grow the oxide layer. This oxide layer was found by ellipsometry to be 1–1.5 nm thick.

Polished p-GaAs wafers with a nominal resistivity of  $1-10^{-3} \Omega\text{-cm}$  were purchased from American Xtal Technology. The samples (1 cm<sup>2</sup>) were treated by a UV-ozonator for 10 min and cleaned as described elsewhere.<sup>42</sup> This treatment was found by ellipsometry<sup>42</sup> to leave a 0.5–1 nm thick oxide layer on the surface.

**2.4. Monolayer Formation.** The molecules were self-assembled onto mercury drops (see section 2.5), forming partially organized monolayers by immersion of the drops in 5 mM ethanol solutions, to which few drops of chloroform were added, for 8 min, followed by immersion in clean ethanol. The same results are obtained for adsorption times of 10 and 60 min. Monolayers can also be adsorbed from pure ethanol and from acetonitrile but this required ultrasonic agitation to get complete dissolution. The adsorption is driven by (i) hydrophobic interactions between the mercury surface and the molecules, (ii) by the intermolecular forces between the long alkyl chains, and (iii)

**Figure 1.** Schematic picture of the solution-free junction: Hg/molecules/SiO<sub>x</sub>-p-Si. The series of disulfide derivatives with different R groups (Scheme 1) was used.

formation of Hg–S bonds. These driving forces and the liquid nature of the Hg provide a reproducible, homogeneous, and defect-free surface. Moreover, because Hg has a high surface tension, the drop and the monolayer formed on it are compliant and can conform to the topography of a solid surface with which it is brought into contact.<sup>43</sup>

**2.5. Junctions and Measurements Setup.** The Hg/molecules/SiO<sub>x</sub>-p-Si junction is illustrated in Figure 1. The cyclic disulfide group served as linker to the Hg drop that was one of the electrodes. The Hg drop was prepared with a commercial, controlled growth, hanging mercury drop (HMD) electrode apparatus manufactured by BAS, United States. The mercury was 99.9999% pure. Typical drop diameters were 0.05 cm.

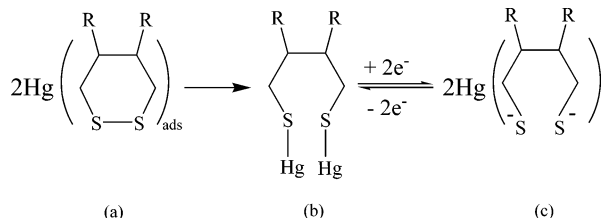
The p-Si/SiO<sub>x</sub> or p-GaAs substrates were mounted on a homemade stage that allowed both coarse and fine movements of the substrate toward the mercury drop. InGa was used to make back contacts to the samples, by scratching their back surface with a diamond knife. This ensured that no significant potential drop developed over this contact. The complete setup was placed on a vibration-free optical Table, which was placed in a class 10 000 clean room that was held at 20 °C and 40% relative humidity. The Hg drop remained steady after the monolayer self-assembled on it. It is important to stress that, in contrast to other work with Hg electrodes,<sup>44,45</sup> our measurements are conducted without any solvent.<sup>46</sup> The contact between the Hg drop and the p-Si/SiO<sub>x</sub> (or p-GaAs) was monitored by an optical microscope. This also allowed the measurement of the actual geometric contact area (~0.05 mm<sup>2</sup>). Current–voltage ( $I$ - $V$ ) characteristics were collected in the voltage scan mode, using an HP 4155 semiconductor parameter analyzer. Applied biases are given as positive when the Hg electrode is negatively biased with respect to the p-Si/SiO<sub>x</sub> substrate. In this situation, (Hg -, Si +) the Hg/p-Si–SiO<sub>x</sub> is forward biased. We used several scan rates, viz., 1, 20, and 30 mV/sec to check the stability of the junction. Deterioration of the monolayer was observed only if very long scans, or/and high voltages (> 2.5–3 V) were used.

**2.6. Electrochemical Characterization. 2.6.1. Evaluation of the Surface Coverage.** Cyclic voltammetry (CV) measurements were conducted in solution. To estimate the surface coverage<sup>47</sup> a hanging mercury drop (HMD) electrode (1 mm<sup>2</sup>) was soaked in 1 mM ethanol

(39) Dunning, T. J. *J. Chem. Phys.* **1989**, *90*, 1007–1023.(40) Kendall, R. A.; Dunning, T. J.; Harrison, R. J. *J. Chem. Phys.* **1992**, *96*, 6796.(41) Bruening, M.; Cohen, R.; Guillemoles, J. F.; Moav, T.; Libman, J.; Shanzer, A.; Cahen, D. *J. Am. Chem. Soc.* **1997**, *119*, 5720–5728.(42) Vilan, A.; Ghabboun, J.; Cahen, D. *J. Phys. Chem. B* **2003**, *107*, 6360–6376.(43) Haag, R.; Rampi, M. A.; Holmlin, R. E.; Whitesides, G. M. *J. Am. Chem. Soc.* **1999**, *121*, 7895–7905.(44) Rampi, M. A.; Whitesides, G. M. *Chem. Phys.* **2002**, *281*, 373–391.(45) Slowinski, K.; Chamberlin, R. V.; Miller, C. J.; Majda, M. *J. Am. Chem. Soc.* **1997**, *119*, 11910–11919.

(46) If the whole system, after assembly, is immersed in DI water or in hexane, (to check for possible influence of residual solvent, esp. on the effects of scan rate and on hysteresis by using a polar and an apolar solvent) essentially the same NDR behavior is observed as for the dry system.

**Scheme 2.** Proposed Mechanism for Reduction of the Cyclic Disulfide Molecules: (a) Molecules Adsorbed on the Hg Electrode with the Disulfide Bond Intact; (b) Molecules Adsorbed after S–S Bond Cleavage and Bound to Hg Atoms on the Hg Surface; (c) Molecules after Reduction (b → c) and, as a Result, No Longer Chemically Bound to the Hg Surface



solution for 60 min.<sup>48</sup> R = CH<sub>3</sub> terminated disulfide molecules were used. After soaking, the HMD electrode was removed from the solution and rinsed with ethanol and deionized water. Because the used molecules are not electrochemically active, “blocking” experiments using reduction of Ru(NH<sub>3</sub>)<sub>6</sub><sup>3+</sup> (1 mM in NaCl solution) on the HMD electrode were done. Ru(NH<sub>3</sub>)<sub>6</sub><sup>3+</sup> is reversibly reduced at the bare HMD at -180 mV (vs Ag/AgCl). When the HMD electrode was covered by the R = CH<sub>3</sub> disulfides-terminated molecules, the Ru(NH<sub>3</sub>)<sub>6</sub><sup>3+</sup> redox peak was still observed, but the current was much smaller. From the change in peak area we estimate a lower limit of 55% coverage by these molecules.<sup>41,49</sup> Based on the relatively large (-4.8 D) dipole moment of the R = CH<sub>3</sub> terminated disulfide molecule, its monolayers will give poorer coverage than those of the other compounds, due to depolarization.<sup>50</sup> However, even at 55% coverage, the high surface tension of the liquid mercury will limit the occurrence of pinholes with the ~2.4 nm long molecules, used here.

**2.6.2. Reductive Desorption of the Molecules.** The reductive desorption peak of the molecules appears at -0.9 V, applied to the HMD electrode (vs Ag/AgCl), with a width of 200 mV. In a second scan, that is, after desorption of the disulfide molecules into the solution, the Ru(NH<sub>3</sub>)<sub>6</sub><sup>3+</sup> reduction peak current increased nearly twofold and the reductive desorption peak was reduced to some 25% of that observed in the first scan. These measurements indicate that the molecules detach from the HMD electrode, if -0.9 V (vs Ag/AgCl) is applied. They also allow another estimate of molecule coverage, by integrating the peak. This yields nearly full coverage, that is, consistent with the 55% lower limit, found above.

### 3. Results and Discussions

Upon applying negative bias to the mercury, the cyclic disulfide end of the molecule can undergo the following redox reaction (Scheme 2):<sup>51,52</sup> The reduction of the Hg–SR bond and its reoxidation, is reversible on Hg, but irreversible on other common electrodes, such as Pt or Au electrodes.<sup>51</sup>

This process can occur at the interface, as no other reagents are needed. The electrostatic screening, normally provided by solvent molecules or counterions, is supplied by the image charge on the metal. The two added electrons are mainly localized on the sulfur atoms.<sup>25</sup> This localization results from the fact that the reduced disulfide bond is not conjugated to the rest of the molecule, and that there is good screening by the metal at that location.

The reaction presented in Scheme 2 plays a key role in this study. After the molecules undergo this redox reaction they are not chemisorbed anymore and their coupling to the Hg dramatically decreases. This leads to a new molecule–electrode interface:

- Absence of a chemical bond between the Hg and the molecule creates an additional potential barrier for electrons (holes), which tunnel through the molecules, from the Hg toward the p-Si/SiO<sub>x</sub> electrode (from the p-Si/SiO<sub>x</sub> toward the Hg).
- Localized charge on the sulfur atoms of the reduced disulfide molecules poses a barrier for charge transport (in any direction).
- Breaking of the Hg–S bond localizes negative charge on the S, with a corresponding positive image charge in the Hg. This forms a positive dipole (negative pole pointing away from the Hg) that opposes electron (holes) flow from the Hg toward the p-Si/SiO<sub>x</sub> (from the p-Si/SiO<sub>x</sub> toward the Hg).

**3.1. I–V Characteristics.** Typical current–voltage (I–V) curves of Hg/molecules/SiO<sub>x</sub>-p-Si are shown in Figure 2. We use a series of disulfide molecules that differ in their end group and, therefore, in their dipole moment (as shown in Table 1). All the devices show NDR at room temperature with a peak (voltage) position variation of ~20%.<sup>53</sup> Devices with Br as the end group have the highest peak to valley ration (PVR)<sup>54</sup> of 3–40 with NDR of 2 Ω/cm<sup>2</sup> (Figures 2a, 5, and 6).

Moreover, they are relatively stable during repetitive voltage scanning, without any reduction in the current or in the effect (Figure 2a; but see section 3.2, below).<sup>55</sup> Devices with R = OCH<sub>3</sub>, CN, or CH<sub>3</sub> as end groups show smaller (OCH<sub>3</sub>), as well as less stable (CH<sub>3</sub>, CN), NDR, with PVR ~ 2–3 (cf. Figures 2b,c, and d). We attribute the differences in stability of the junctions to the molecules’ dipole moments, as discussed in section 3.3. The relatively high PVR value observed with R = Br compared to the others is likely due to a better organization of the molecules before and after the reduction process, which is made possible by their modest dipole moment (Table 1).<sup>25</sup>

Differences in current densities are observed between experiments and between junctions with different molecules. Much of the experimental variability between junctions with the same molecules stems from variations in the SiO<sub>x</sub> thickness, which affects the tunneling transmission probability. Consistent differences are found between R = CH<sub>3</sub> and R = OCH<sub>3</sub> systems. The ~3× higher currents for the former are likely due to the wider tunneling barrier presented by the OCH<sub>3</sub>-terminated molecular layer.<sup>56–58</sup> Other factors can affect the tunneling barrier apart from the barrier width, such as the molecules’

(47) Muskal, N.; Turyan, I.; Mandler, D. *J. Electroanal. Chem.* **1996**, *409*, 131–136.

(48) Monolayer preparation conditions for the dry NDR and the wet electrochemistry experiments were slightly different, in terms of time, concentration, and solvent. We checked that this does not affect the results by confirming that NDR experiments with samples prepared by 60 min of soaking in 1 mM ethanol solution gave the same results as those reported here. We note that for thiols it is known that full coverage is achieved after less than 5 min for thiol concentrations above 10<sup>-5</sup> M (cf Muskal et al.<sup>47</sup>). Monolayer rearrangement (and ordering) then occurs after initial adsorption. This can be outside the solvent (as for the dry NDR measurements) or in the solvent (as for the wet electrochemistry experiments). For the dry measurements, we preferred shorter adsorption times to minimize solvent exposure as this improved reproducibility. For the wet electrochemistry measurements this was not an issue.

(49) Coverages of 75–100% were found for the small disulfides, used in Bruening et al.,<sup>41</sup> on Au and of 75% for a disulfide with one palmitoyl group.

(50) Gershewitz, O.; Grinstein, M.; Sukenik, C. N.; Regev, K.; Ghabboun, J.; Cahen, D. *J. Phys. Chem. B* **2004**, *108*, 664–672.

(51) Stankovich, M. T.; Bard, A. J. *J. Electroanal. Chem.* **1977**, *75*, 487–505.

(52) This proposed mechanism is based on the one for binding cystine to mercury in solution, given in Stankovich et al.<sup>51</sup>

(53) This is probably due to variations in the thickness of the SiO<sub>x</sub> layer.

(54) The PVR value is the ratio of the peak and the valley currents that occur at the beginning and the end of the range over which the system shows negative differential resistance.

(55) The time delay between each voltage scan was 2 min.

(56) We assume that the tunneling barrier with monolayers of molecules with R = OCH<sub>3</sub> is about 0.2 nm wider than that for molecules with R = CH<sub>3</sub>.

(57) Simmons, J. G. *J. Appl. Phys.* **1964**, *35*, 2655.

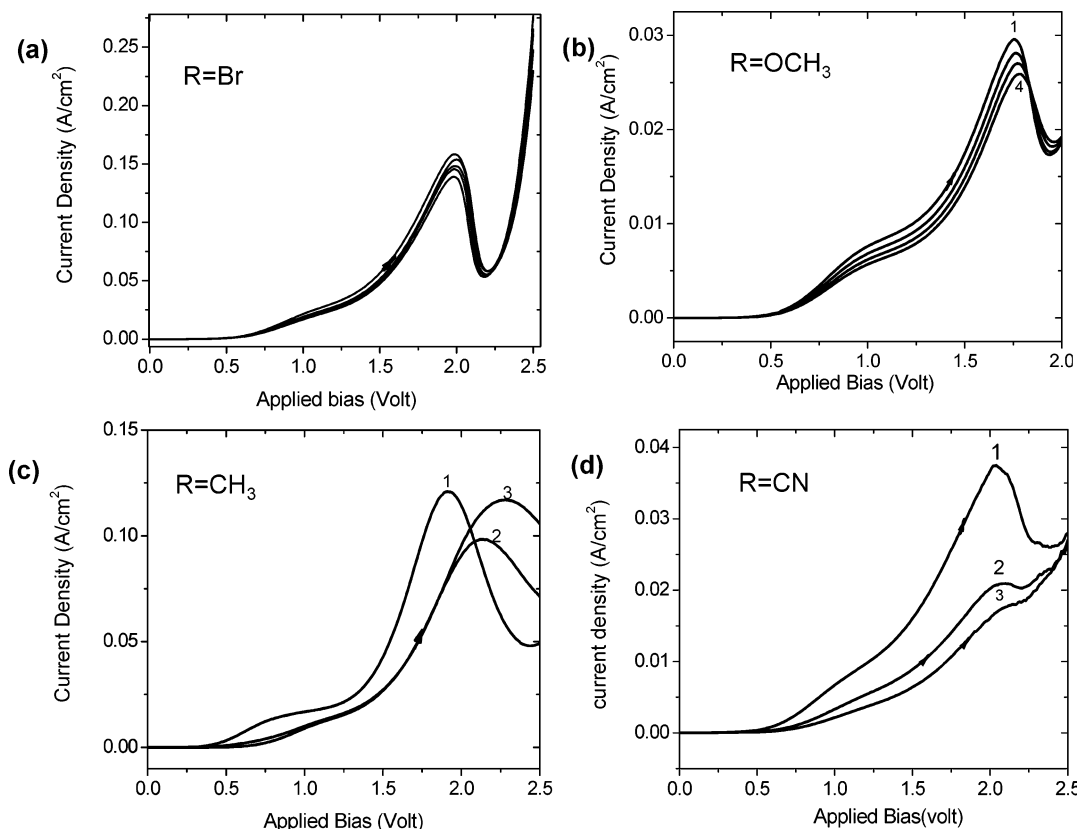


**Figure 2.** Current (density)–voltage characteristics for the Hg/molecules/SiO<sub>2</sub>–p-Si junctions, with different end-group molecules. Numbers next to the plots indicate sequence of scans. All scans are from low to high voltage.<sup>55</sup> The best NDR behavior was observed with R = Br (a) and with R = OCH<sub>3</sub> (b). For (a) the NDR stabilizes at the higher peak value than for (b). With R = CH<sub>3</sub>(c) and, especially, R = CN (d), poor and less stable or unstable NDR behavior is obtained. Scan direction is from low to high voltage; scan rate: 20 mV/sec; junction area: 0.05 mm<sup>2</sup>.

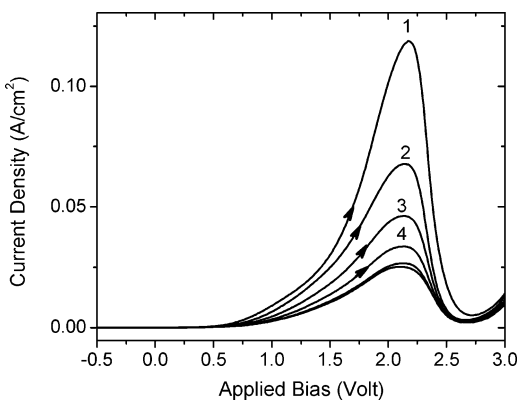


**Figure 3.** As Figure 2a but with about 20 s delay between the scans. Numbers next to the plots indicate the sequence of scans.

dipole moments and their coupling to the Si/SiO<sub>x</sub> substrate. All of these can influence the resulting potential profiles of the junction within the experimental variability that we observe.

**3.2. Relaxation Time of the System.** Repetitive voltage scanning over the same junction, without any time delay<sup>59</sup> between the measurements, reduces the NDR, also for the stable device with Br as end group, as shown in Figure 3. However, a delay of 2 min between successive measurements (scans) restores the NDR effect without any reduction in the current or

in the effect (Figures 2a and 5b). Apparently, 2 min is the time that the system needs to reorganize, by having the molecules bind again to the mercury electrode and by restoring optimal intermolecular interaction between the chains. Such reorganization may take place also in a dry state.<sup>60</sup>

**3.3. Stability of the System.** The stabilization and the organization of the system is a very important issue in this study, as is shown in Figure 3 and Figure 2. When the molecules undergo the redox reaction, (Scheme 2) they not only lose their chemical bond to the mercury; their dipole moment is changed due to the extra charges on the disulfide part of the molecule. This may affect the organization of the monolayer, as molecules may flip or disorient in order to reduce the dipole–dipole repulsion force at the interface.<sup>50</sup> Indeed, in our preliminary study we could not stabilize the system as we used short length molecules.<sup>25</sup> Here we use molecules with a long alkyl chain (14 carbons). The increase of alkyl-chain-length results in a more organized monolayer that has more van der Waals interactions. These interactions keep the organization of the monolayer, even after detachment of the molecules from the mercury. Yet, as shown in Figure 2d, devices with R = CN terminated molecules were unstable. That is, one can easily see deterioration of the effect within the voltage scans. The calculated dipole moments for the CN- and CH<sub>3</sub>-terminated molecules are large; therefore, it is reasonable that dipole–dipole repulsion<sup>50</sup> leads to adsorption of a disoriented and unorganized monolayer. In fact, the lowest dipole moment is calculated for the R = Br terminated

(58) We calculate the tunneling current using Simmons' model<sup>57</sup> with barrier widths of 3.9 and 4.1 nm (~2.4 nm for the molecule length and ~1.5 nm for the SiO<sub>x</sub> layer). The simulations show that the tunneling current is 8 times lower for the wider barrier.

(59) We define a delay time as the interval time between sequences of voltage scans.

(60) Ulman, A.; Evans, S. D.; Shnidman, Y.; Sharma, R.; Eilers, J. E. *Adv. Colloid Interface Sci.* **1992**, *39*, 175–224.

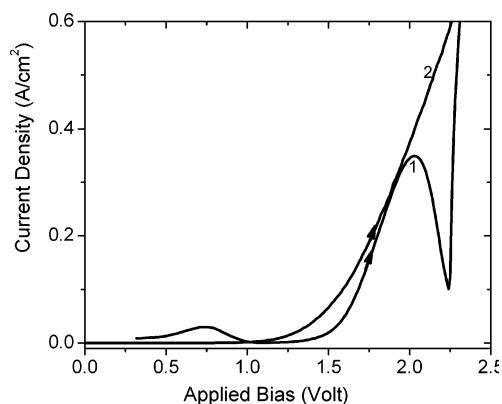


**Figure 4.** Current (density)-voltage characteristics for the p-GaAs/molecules/Hg junction. Other details are as for Figure 2. Numbers next to the plots indicate the sequence of scans, with  $R = \text{CN}$ . Other substituents have shown similar or poorer first-scan NDR. No NDR remained after 1–2 scans. The current density is higher than in Figures 2 and 3, due to the smaller oxide layer on p-GaAs than on Si.

molecules. These give the most stable devices, followed by the  $R = \text{OCH}_3$  devices.

From the reaction illustrated in Scheme 2 it is plausible that the same phenomena will also be observed with simple alkanethiols onto Hg. Indeed, we also observed irreversible NDR behavior with other sulfide-based molecules such as decanethiol. However, for these relatively short molecules the reduction potential already falls in the voltage region where electric breakdown of these molecular junctions occurs ( $\sim -2 \text{ V}$ ).<sup>61</sup> Therefore, for these molecules the reduction process in the solid-state junction is irreversible. For longer-chain thiols breakdown occurs before the reduction potential is reached.

Instability was also observed when we replaced p-Si/SiO<sub>x</sub> by p-GaAs, as shown in Figure 4. The NDR behavior in these systems disappeared after the first voltage scan for all the molecules, without any recovery of the system. Since disulfide molecules can also adsorb onto p-GaAs,<sup>62</sup> it is plausible that detachment of the molecules from the Hg surface leads to readsorption, not only on Hg but also on the p-GaAs surface to reduce dipole-dipole repulsion.<sup>50</sup>

**3.4. Hysteresis.** Figures 5a and b show cyclic voltage scans of the system. As can be seen in (a) NDR in the reverse scan direction is significantly poorer, with a lower PVR value, than that in the forward one. However, as shown in (b) it returns again in the next forward scan, with the same dependence on the time delay as was shown for the unidirectional scans in Figures 2 and 3. We can postulate that applying high voltage to the system (in the reverse scan) results in fast reduction and detachment of the molecules in contrast to the gradual reduction if we scan from low to high voltage. This means that when we apply high negative voltage to the mercury, the current is blocked at once and not gradually; therefore lower PVR values were also observed with just reverse scans. No negative current is observed during the reverse scans, which means that no charge is stored. Rather, it is likely that reduction takes place while the charge passes through the molecules.

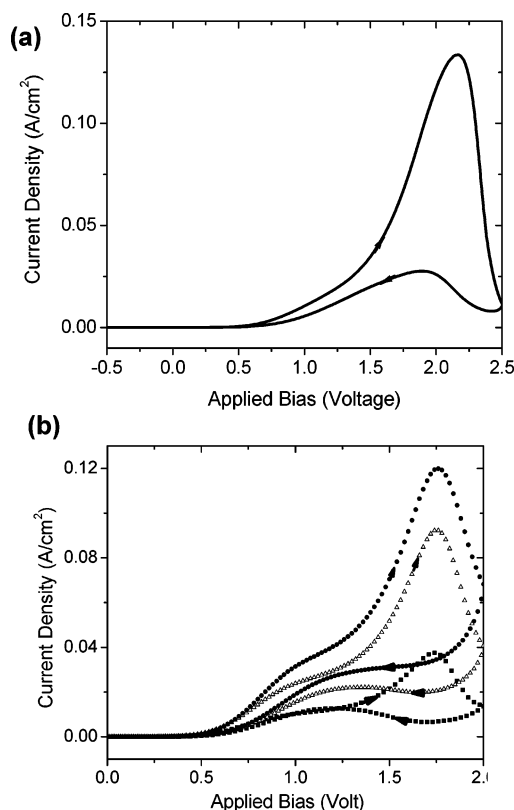


**Figure 5.** (a) Continuous current (density)-voltage characteristics for the Hg/molecules/SiO<sub>x</sub>-p-Si junction with  $R = \text{Br}$ . The PVR value for the forward scan is about 10, whereas for the reverse scan it is about 2. (b) As (a), without any delay time between scans 1 (open triangles) and 2 (solid squares), but with a 2-min delay between scans 2 and 3 (solid circles). Other details are as for Figure 2.

**3.5. Voltage Peak Position.** While there is some variability in the NDR voltage peak position, which we ascribe to the solid-state nature of the system and to the voltage drop over the SiO<sub>x</sub> layer, the range of variability is sufficiently small to allow a meaningful discussion of its position.

We argue that the NDR behavior is due to the reduction process of the disulfide molecules and their detachment from the Hg electrode. If this is so then we can expect the voltage peak positions in solid-state junction and in solution electrochemical measurements to be comparable. Cyclic voltammetry measurements of Hg electrodes, covered with  $R = \text{CH}_3$  molecules, show that these molecules are reduced and detached from the Hg electrode around  $-0.9 \text{ V}$  vs the Ag/AgCl electrode. The Ag/AgCl standard reference potential corresponds to a work function of  $-4.75$  to  $-4.95 \text{ eV}$ .<sup>63,64</sup> This value is very similar to the work function of p-Si and that of thiol-covered Hg.<sup>65</sup> Since the solution contains a relatively concentrated electrolyte, we can neglect the potential drop over it. Thus, when a voltage of  $-0.9 \text{ V}$  is applied between the Ag/AgCl reference electrode and the sulfide-covered Hg one, this will be roughly the potential drop over the molecular layer.<sup>66</sup>

(61) Holmlin, R. E.; Haag, R.; Chabinyk, M. L.; Ismagilov, R. F.; Cohen, A.; Terfort, A.; Rampi, M. A.; Whitesides, G. M. *J. Am. Chem. Soc.* **2001**, *123*, 5075–5085.

(62) Gartsman, K.; Cahen, D.; Kadyshevitch, A.; Libman, J.; Moav, T.; Naaman, R.; Shanzer, A.; Umansky, V.; Vilan, A. *Chem. Phys. Lett.* **1998**, *283*, 301–306.

(63) Stuve, E. M.; Krasnopoler, A.; Sauer, D. E. *Surf. Sci.* **1995**, *335*, 177–185.

(64) Trasatti, S. *Electrochim. Acta* **1991**, *36*, 1659–1667.

(65) The contact potential difference (CPD) between Hg without molecules and p-Si/SiO<sub>x</sub> is about 0.5 V. After adsorption of the molecules the CPD decreases to  $< 0.2 \text{ V}$ .<sup>6</sup>

(66) Cyclic voltammetry measurements were done only with  $R = \text{CH}_3$ -terminated disulfide molecules. We assume that the reduction potential for the other molecules in the series is similar.

As shown in Figure 2, with the solid-state junctions the voltage peak position is around 1.8–2 V (Hg negatively biased). The solid-state junction consists of the molecular monolayer and an additional  $\sim 1.5$ -nm insulating  $\text{SiO}_x$  layer over which some of the applied potential drops. Taking into account the dielectric constants of both the  $\text{SiO}_x$  and the molecular layer, we calculate that about half of the applied voltage drops over the molecular layer.<sup>65,67,68</sup> That is, an applied voltage of 1.8–2 V results in a 0.9–1 V potential drop over the molecular layer. This means that the voltage peak position in the solid-state junction agrees well with the reduction potential of the molecules in solution.

To complete our argument, we now also consider the voltage peak position in our earlier study where we used shorter ( $\sim 1.2$  nm) cyclic disulfide molecules in the same type of solid-state junctions. There, the NDR voltage peak position was around  $-0.8$  V (Hg negatively biased). That is, the reduction of the Hg–S bond as illustrated in Scheme 2 occurred around this voltage. In the present study, we use much longer molecules of  $\sim 2.4$  nm. According to Muskal et al.<sup>47</sup> the reduction potential of alkanethiols shifts to more positive potential with decreasing alkyl chain length. Thus, the reduction potential of the shorter molecules should be more positive than that of the longer molecules (and similar to that of cystine,<sup>69</sup> which is about  $-0.5$  V vs Ag/AgCl).<sup>51</sup> This potential shift is adequately explained by hydrophobic interactions and lateral intermolecular forces between hydrocarbon chains that contribute  $-4.8$  kJ/mol/ $\text{CH}_2$  to the overall stability of *n*-alkyl thiolate films in aqueous solution as well as in the solid state.<sup>34,70</sup> Thus, in our earlier study the NDR voltage peak position should be shifted to more positive potentials, compared to the longer molecules used now, because of their shorter length and because they can form only a partially organized monolayer. The  $\sim -0.8$  V voltage peak position for the shorter molecules corresponds to an  $\sim -0.4$  V potential drop over the molecular layer, because about half of the potential drops over the  $\text{SiO}_x$  layer. If we now calculate the potential drop over the Hg–S bond for the short and the long molecules, we find that the potential drop over the Hg–S bond is comparable if  $\sim -0.8$  V is applied to the short molecules or  $\sim -2$  V to the longer ones.<sup>71</sup>

Since the NDR behavior is controlled by an electrochemical reaction at the molecule–electrode interface, the voltage peak position should depend on the voltage scan rate. Figure 6 shows the *I*–*V* characteristics for different voltage scan rates. A fast scan rate of 30 mV/sec shifts the peak to higher voltage and a

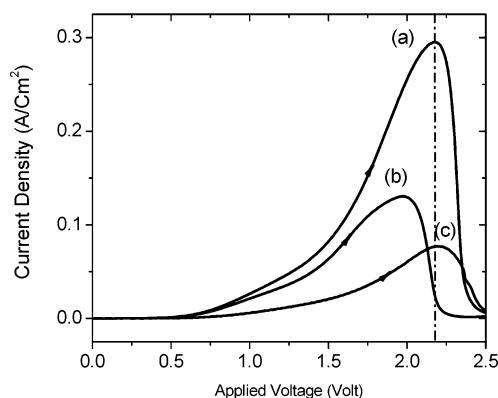


**Figure 6.** Current (density)–voltage characteristics for the Hg/molecules/ $\text{SiO}_x$ -p-Si junction with R = Br. (a) Medium scan rate of 20 mV/sec (PVR = 40); (b) slow scan rate of 1 mV/sec; (c) fast scan rate of 30 mV/sec. The other details are as for Figure 2.

slow scan rate of 1 mV/sec shifts it to lower voltage. The highest PVR was observed at a “medium” scan rate of 20 mV/sec. A possible explanation for this observation is that fast scanning results in partial reduction of the molecules, while for slow scanning all the molecules may be reduced. However, they might be damaged because of the continuing high electric field over them. Thus, while the reduction of the molecules, which controls the action of the device, relies on thermodynamic considerations, the deterioration of the molecules is also kinetically controlled.

**3.6. Low-Voltage Behavior.** Two distinct types of NDR are observed with negatively biased Hg (see Figures 2 and 6). The low voltage feature mostly appears as a plateau and was observed for all disulfides molecules. Such feature was observed in cyclic voltammetry of cystine (RSSR) on Hg in solution.<sup>51,72,73</sup> There it was suggested that the mechanism for the low voltage feature involves reaction of RSSR with Hg leading to cleavage of the disulfide bond. For the short molecules system we did not observe any NDR-like behavior at more positive voltage than its reported NDR behavior. This is because at  $V < -0.5$  the voltage is less than the barrier height of the junction.<sup>25</sup> Therefore, over that voltage range the metal/semiconductor junction will still be rectifying, and the current that passes through the junction will be very small.

As described in section 3.9, irreversible NDR behavior in the same voltage region was also observed for systems without an Hg–S bond. Therefore, we are careful to attribute the pre-NDR behavior to the nature of the molecules.

**3.7 High-Voltage *I*–*V* Characteristics.** Within the model that we present to explain the NDR, at voltages higher than those required for the NDR feature, the system is composed of a junction in which the molecules are not chemically bound anymore to either side of the electrodes. As a result, the current in that range is expected to be less reproducible than at lower voltages where the molecules are chemically bound to the Hg electrode.<sup>7</sup> In the absence of such chemical bonds, the monolayer’s organization will be less controlled than when the molecules are bound to the Hg. Apart from the problem of possible damage to the monolayer molecules at these high voltages, in this voltage range their organization depends only on the van der Waals interaction between the chains. Thus, we postulate that the details of the *I*–*V* characteristics of the junction at voltages higher than the NDR ones are influenced

(67) We took 3.8 and 4.5 as the dielectric constants of the  $\text{SiO}_x$  and of the molecular layer, respectively. 1.5 nm was taken as the thickness of the  $\text{SiO}_x$  and 2.5 nm as the length of the molecules.

(68) Since one side of the interface is a semiconductor, extra charge at the interface will normally lead to realignment of the semiconductor energy band positions, with respect to the metal Fermi level. This will change the band bending and the barrier height for electron transport from the metal toward the semiconductor. However, here the reduction reaction occurs at forward bias potentials that are much higher than the barrier height, which means that no depletion layer is left in the semiconductor. Therefore, we can assume that the observed NDR does not result from changes in the metal/semiconductor barrier heights.

(69) Cystine is a short amino acid of RSSR type, with R =  $\text{C}_3\text{H}_6\text{O}_2\text{N}$ .

(70) Stevenson, K. J.; Mitchell, M.; White, H. S. *J. Phys. Chem. B* **1998**, *102*, 1235–1240.

(71) The potential profile was estimated by imposing continuity on the mercury/ $\text{SiO}_x$ -p-Si interface as a boundary condition. The same dielectric constant of 4 for the  $\text{SiO}_x$  and the molecular layer (this time without S) was taken for the sake of simplicity, 1.5 nm as the  $\text{SiO}_x$  length, 1.2 and 2.4 nm as the lengths of the short and the long molecules (without S), respectively. For the Hg–S bond we took 5.5 as the dielectric constant and 0.25 nm as the bond length.

(72) Koryta, J.; Pradac, J. *J. Electroanal. Chem.* **1968**, *17*, 177–183.

(73) Koryta, J.; Pradac, J. *J. Electroanal. Chem.* **1968**, *17*, 185–189.



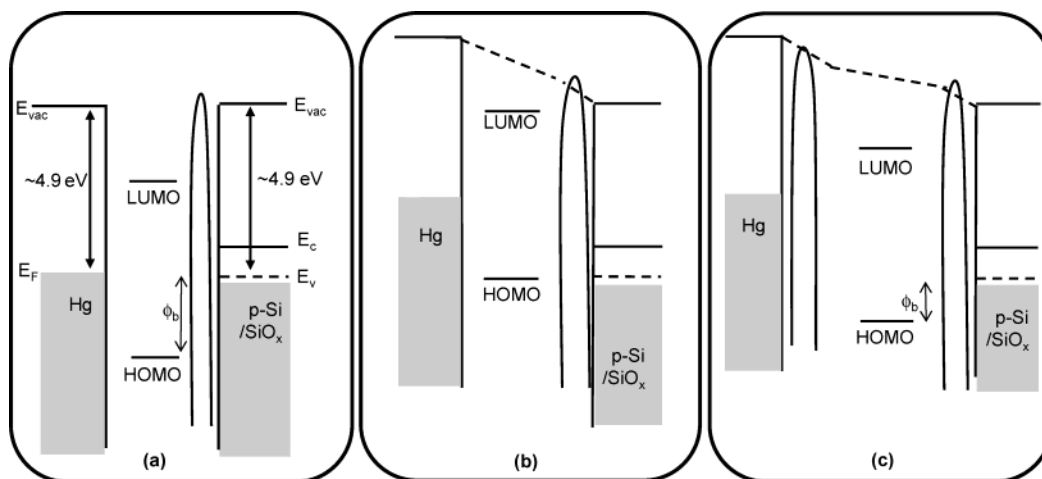


**Figure 7.** Energy levels and band diagrams of the Hg/molecules/SiO<sub>x</sub>-p-Si junction.<sup>65</sup> The following energy levels are shown:  $E_F$ , Fermi level of the electrodes;  $E_{vac}$ , vacuum level;  $E_v$ , top of the valence band;  $E_c$ , bottom of the conduction band.  $\phi_b$  is the tunneling barrier for electron transport through the HOMO, often referred to as hole tunneling. This is likely associated with the Hg-S bond before bond breakage and with the sulfur lone-pair orbital after bond breakage.<sup>77</sup> (a) After electrical contact at  $V = 0$ ; (b) under forward bias at  $V = 2$  (Hg is negatively biased), when the molecules may undergo the reduction process; (c) after the redox reaction of the molecules and their detachment from the Hg surface.<sup>78</sup> The potential drops mainly across the newly formed insulating barrier at the molecule/mercury interface. Therefore, the alignment of the molecular energy levels with respect to the Hg is changed.

by the organization of the unbound monolayer. Indeed, Haran et al.<sup>74</sup> found more efficient charge transport the better organized the monolayers.

Experimentally we find that the  $I$ - $V$  characteristics at voltages beyond the NDR ones, as presented in Figures 2a and 3, represent extreme cases of behavior, with most of the  $I$ - $V$  curves showing behavior intermediate between these two. We assume that systems such as the one for which  $I$ - $V$  curves are shown in Figure 2a remain better organized than those with the curves shown in Figure 3. In this voltage range we do not control a priori which will give what.

If we examine Figure 3 carefully and compare the valley features between the different voltage scans, we see that in the last scan the valley's voltage range is wider than in the first one, indicating that the unbound monolayer is now less organized than that obtained during the first scan. The same holds for reverse scanning; that is, the valley's voltage range for the high-to-low voltage scan is much wider than that for the low-to-high voltage one for the same device (Figure 5), indicating, as expected, a less-organized monolayer during the high-to-low voltage scanning.

**3.8. Proposed Mechanism.** The NDR device can be viewed as a "mixture" of two different junctions that are dissimilar at the molecule-electrode interface and therefore in their  $I$ - $V$  characteristics: The first junction exhibits relatively high currents (low barrier height) since the molecules are chemically adsorbed onto the mercury electrode. The second junction exhibits lower currents mainly due to a missing of the chemical bond between the molecules and the mercury. As we increase the applied bias, more molecules are reduced. Therefore, charge transmission becomes less efficient and the  $I$ - $V$  curve is the one that characterizes the second junction, in which less current passes for a given voltage. This yields the NDR behavior. Following this rationalization, the PVR value actually reflects the conductance ratio between these two types of junctions mentioned above. The conductance difference between these two junctions is attributed to the broken Hg-S bond in the

second junction and to dipole changes at the interface resulting from reduction of the molecules. This yields the approximately one order of magnitude difference in current (the  $\sim$ PVR value for R = Br). Qualitatively, this fits other studies, where a missing chemical bond at the molecule-electrode interface was shown to result in order(s) of magnitude reduction in the current.<sup>5-9</sup>

We note that the NDR behavior is often ascribed to resonance tunneling. If resonance tunneling were the main mechanism here, NDR behavior should have also occurred for a system of opposite polarity.<sup>18</sup> This was not the case; that is, we did not observe NDR behavior for Hg/molecules/SiO<sub>x</sub>-*n*-Si systems, with Hg positively biased with respect to the *n*-Si/SiO<sub>x</sub> substrate.

**3.8.1. Energy Band Diagram.** The energy band diagram of the Hg/molecules/SiO<sub>x</sub>-p-Si junction under applied bias is illustrated in Figure 7. We shall follow the convention that the p-Si/SiO<sub>x</sub> electrode is always grounded and its Fermi level can be used as the reference energy. A negative potential applied to the Hg electrode shifts its Fermi level to higher absolute energies. Since the molecules are adsorbed onto the mercury surface and detach from the p-Si/SiO<sub>x</sub> electrode, the molecular energy levels, the lowest unoccupied molecular orbital (LUMO), and the highest occupied molecular orbital (HOMO) follow the Hg energy bands and go up in absolute energy as well. The energy shift of the LUMO/HOMO relative to the energy levels of the p-Si/SiO<sub>x</sub> electrode is determined by the ratio of the voltage drop over the molecular layer (including the potential drop over the Hg-S bond), and that over the insulating barrier at the molecule/p-Si-SiO<sub>x</sub> interface.<sup>75,76</sup> That is, the potential profile of the junction plays an important role in determining the alignment of the molecular energy levels relative to the Fermi energy levels of the electrodes. Increasing the (negative) voltage, applied to the junctions, decreases the barrier for hole tunneling (electron transport via the HOMO) from the p-Si/SiO<sub>x</sub> toward the Hg electrode (Figure 7b). We presume that at  $\sim -2$  V (Figure 7b) the HOMO level is close to resonance

(74) Haran, A.; Waldeck, D.; Naaman, R.; Moons, E.; Cahen, D. *Science* **1994**, *263*, 948-950.

(75) Taylor, J.; Brandbyge, M.; Stokbro, K. *Phys. Rev. Lett.* **2002**, *89*, 138301.  
(76) Kornilovitch, P. E.; Bratkovsky, A. M.; Williams, S. R. *Phys. Rev. B* **2002**, *66*, 165436.

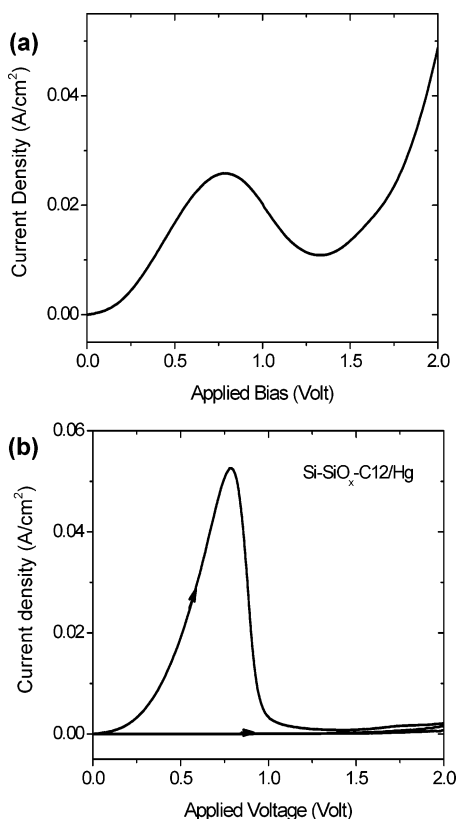


**Figure 8.** Examples of an unstable NDR in different systems. (a) p-Si-SiO<sub>x</sub>/CS<sub>2</sub>/Hg; (b) p-Si-SiO<sub>x</sub>/dodecyltrichlorosilane/Hg. Other details as for Figure 2.

with the Fermi level of the Si/SiO<sub>x</sub>. Then, the molecules can undergo the reduction process that results as their detachment from the mercury electrode. Hence, an insulating barrier for charge transport at the molecular layer/Hg interface is formed (Figure 7c). This leads not only to a wider barrier for charge tunneling but also to a different potential profile of the junction. Thus, the potential drops mainly over the insulating barriers at the molecular layer/electrode interface and barely over the molecular layer. Therefore, the molecular levels are pushed down in absolute energy compared to their previous alignment (Figure 7c). Now the barrier for tunneling,  $\phi_b$ , is not only wider, but also higher, as can be seen from the band diagram (cf. Figure 7c with 7b). This obviously reduces the observed current.

**3.9. Other Systems with Unstable NDR Effect.** NDR behavior within this setup, that is, a solution-free, Hg electrode junction, was sporadically observed with different junctions with other molecules and/or electrodes, if sufficiently low current passed in the bias direction favorable for reduction (metal electrode negative). However, this behavior was mostly irreproducible and unstable. That is, the peak disappeared after the first or the second voltage scanning, without any recovery of the system. The voltage peak position or a plateau for all these junctions was observed around 0.6–0.8 V. Different types of molecules were adsorbed and assembled onto one of the electrodes: dodecyl trichlorosilane, hexadecyl trichlorosilane and octadecyl trichlorosilane onto p-Si/SiO<sub>x</sub>, fullerene derivatives, as well as CS<sub>2</sub> onto Hg. Some of the resulting  $I$ – $V$  curves are shown in Figure 8. Unstable NDR-like  $I$ – $V$  behavior in this lower voltage range is also seen in the currently studied systems that yield the reproducible NDR effect (cf. Figures 2, 4, and 5b). Since the low voltage effect was observed at similar

voltages for different types of molecules, it is evidently not just related to the molecules. Moreover, the  $I$ – $V$  derivatives for the Hg/p-Si and Hg/p-Si–SiO<sub>x</sub> junctions also show nonlinear behavior (plateau) around 0.8 V. Thus, we postulate that such effects are due to reduction processes (“background” current) onto the mercury surface, which contribute some component to the total current. Such processes will not be observed when the measured current is relatively high. Therefore, one can miss it while doing reference measurements (without molecules). This argument is also valid for other systems, such as for Au and Pt electrodes, which can also undergo oxidation/reduction at relatively low voltages. For example, the oxidation of cystine on Au is observed in the potential region of formation of a Au surface oxide and the current peak has the same potential as the peak of the surface oxide formation.<sup>72</sup> Thus, while we did occasionally observe NDR-like behavior with Au electrodes, this was neither repeatable nor reproducible. Therefore, it is not clear in how far such a behavior can be attributed to the molecular properties.

#### 4. Conclusions and Outlook

Stable NDR was obtained with molecules that were synthesized based on our earlier experience with unstable NDR results.<sup>25</sup> These results have indicated the importance of maintaining the monolayer organization, to allow rebinding of the molecules that were disconnected from the electrode by the reduction of the S bond. The new compounds were modified by inserting long alkyl-chain moieties in the molecules that stabilized the organization of the monolayers.

In this paper, we did not only show that molecule–electrode interactions at the contact interfaces are central for device action, but also demonstrated that it is possible to get some control over these interactions. It is thus probable that the most important conclusion of this work is that for molecule-based devices, the chemistry at the molecule–electrode interface should be considered as much as the electrical properties of the molecule itself should be. Additionally, the ability to control the properties at the molecule–electrode interface will enable the design and building of devices based on the molecule’s signature itself. The work presented here points to an alternative concept in molecular rectification and smart molecular electronics devices (cf. recent theoretical work);<sup>79</sup> that is, by establishing an insulating barrier at the molecule–electrode interface during the voltage scan or, by creating a dipole layer at the molecule–electrode interface, one can get nonlinear  $I$ – $V$  characteristics.

**Acknowledgment.** We are grateful to Drs. L. Echegoyen and F. Song (Clemson University) for the wet electrochemical measurements, to Prof. Jan M. L. Martin and Mr. Mark Iron (Org. Chem. Department, Weizmann Inst.) for their guidance and help, respectively with the quantum chemical calculations and their interpretations, and to Ms. R. Lazar for skillful technical assistance in the synthesis of the cyclic disulfide molecules. We thank Drs. Y. Selzer and D. Bonifazi, and Mr. S. Ruehle for useful discussions. We acknowledge partial support from the Israel Science Foundation.

JA049584L

(77) Alloway, D. M.; Hofmann, M.; Smith, D. L.; Gruhn, N. E.; Graham, A. L.; Colorado, R. J.; Wysocki, V. H.; Lee, R.; Lee, P. A.; Armstrong, N. R. *J. Phys. Chem. B* **2003**, *107*, 11690–11699.

(78) Because of the negative charges on the disulfide molecules after bond breaking and reduction, their HOMO–LUMO gap will decrease.

(79) Troisi, A.; Ratner, M. A. *J. Am. Chem. Soc.* **2002**, *124*, 14528–14529.